Graphical Abstract

Fast Statistical Homogenization Procedure for estimation of effective properties of Ceramic Matrix Composites (CMC) with random microstructure

Marco Pingaro, Maria Laura De Bellis, Emanuele Reccia, Patrizia Trovalusci, Tomasz Sadowski

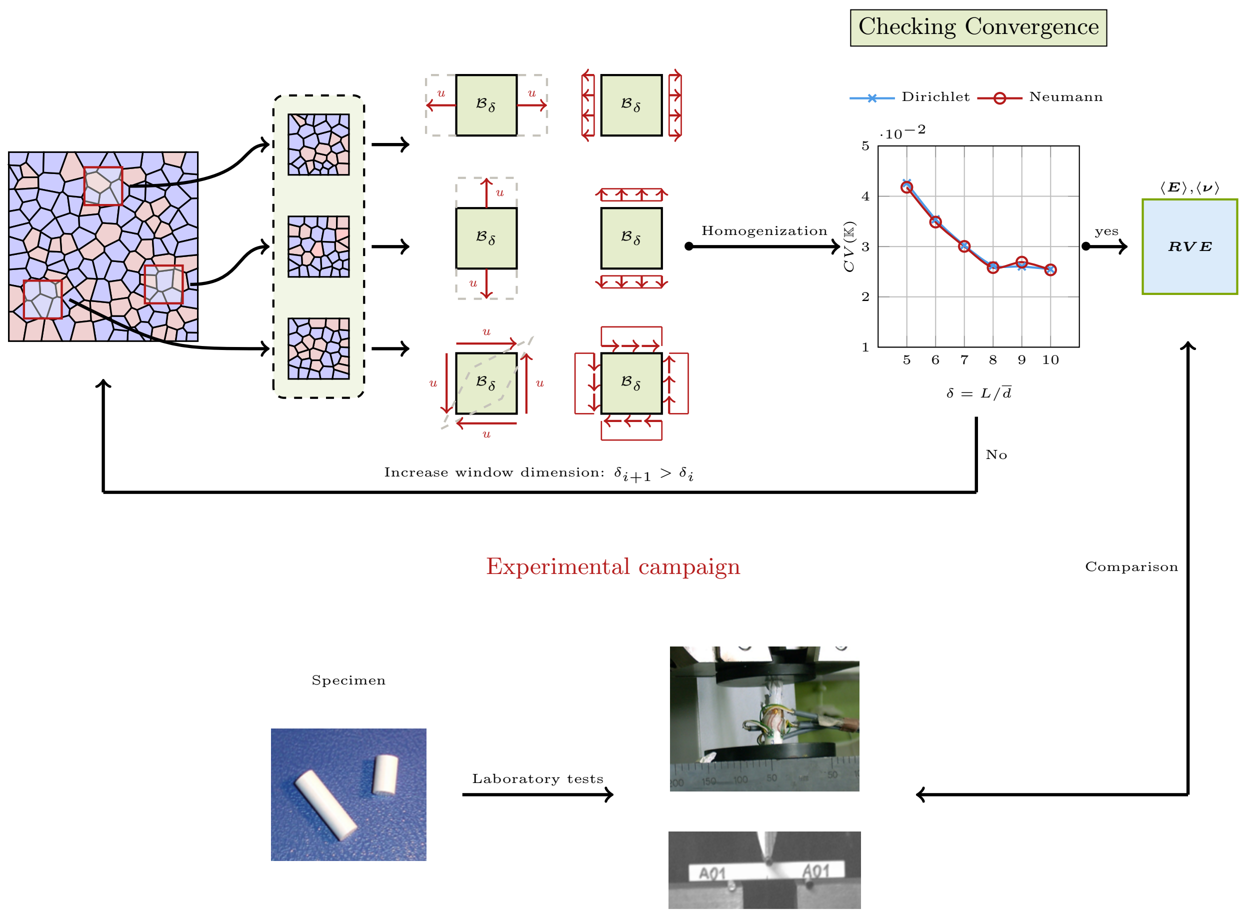

Highlights

Fast Statistical Homogenization Procedure for estimation of effective properties of Ceramic Matrix Composites (CMC) with random microstructure

Marco Pingaro, Maria Laura De Bellis, Emanuele Reccia, Patrizia Trovalusci, Tomasz Sadowski

- Homogenization of random Ceramic Matrix Composites (CMC)
- Fast identification of the homogenized moduli with the Virtual Element Method
- Parametric analysis

Fast Statistical Homogenization Procedure for estimation of effective properties of Ceramic Matrix Composites (CMC) with random microstructure

Marco Pingaro, Maria Laura De Bellis, Emanuele Reccia, Patrizia Trovalusci, Tomasz Sadowski

[a] *Department of Structural and Geotechnical Engineering, Sapienza University of Rome, Via Antonio Gramsci 54, Rome, 00197, Italy,*
[b] *Department of Engineering and Geology, Gabriele d'Annunzio University, Viale Pindaro 42, Pescara, 65122, Italy,*
[c] *Department of Civil and Environmental Engineering and Architecture, University of Cagliari, Via Marengo 2, Cagliari, 09123, Italy,*
[d] *Department of Structural and Geotechnical Engineering, Sapienza University of Rome, Via Antonio Gramsci 54, Rome, 00197, Italy,*
[e] *Department of Solid Mechanics, Lublin University of Technology, ul. Nadbystrzycka 40, Lublin, 20-618, Poland,*

Abstract

The modern polycrystalline composite materials have a complex internal structure consisting of different phases and interfaces with random distribution. Relevant examples are Al_2O_3/ZrO_2, i.e. alumina/zirconia composites, widely used as structural materials with applications ranging from aerospace to bio-engineering. Depending on the phases content and on the grain size a broad range of material characteristics, among which elastic constants, can be obtained.
With the aim of characterizing this class of materials, we exploit a numerical Fast Statistical Homogenization Procedure (FSHP) in order to both estimate the size of the Representative Volume Elements (RVE) and the effective elastic properties, assuming a linear elastic material behaviour.
The 2-D analyses are performed considering a microstructure inspired by images of real portions of the Al_2O_3/ZrO_2 composite obtained from a scanning electron microscope. The recent Virtual Element Method is used in combination with the FSHP approach to numerically solve boundary value problems. Different volume contents of phases are considered ranging from pure Alumina to pure zirconia. The results are useful to reliably characterize

such materials in the elastic range taking into account the role played by random distribution of grains.

Keywords: Ceramic materials, Random materials, Homogenization, Virtual Element Method

1. Introduction

Ceramic matrix composites (CMCs) are a wide class of composites made either by ceramic particles or short/long fibers randomly embedded in a ceramic matrix, or even polycristalline or also layered composites. They have been designed to overcome the well-known limitations exhibited by standard ceramics used in technical applications, especially related to fragile fracture behaviour both in the presence of mechanical or thermal loads [1]. The addition of ceramic particles or fibers has, indeed, the beneficial effect of increasing the fracture toughness, possibly causing a transition from a fragile to a ductile fracture, and increasing the thermal shock resistance of the composite. On the other hand, the composite material still retains the positive characteristics of the ceramic matrix such as the high strength and Young modulus. Applications include heat shield systems for space vehicles, brake disks, slide bearings, components for high-temperature gas turbines, cutting tools and components for burners, among others [2, 3, 4, 5].
A noteworthy example of a polycrystalline CMC certainly is alumina and phase-stabilized zirconia Al_2O_3/ZrO_2 (with different volume contents), see [6]. The considered composite strikes a good balance between positive features of both alumina, i.e. high hardness and low age susceptibility, and zirconia, i.e. high fracture toughness and resistance to subcritical crack growth, see [7, 8]. The Al_2O_3/ZrO_2 composite is characterized by a complex internal structure in which grains of either alumina or zirconia of different sizes (ranging from 0.2μm to 2μm) are randomly distributed to form a polycrystal (see Fig.1). Its mechanical characterization has aroused much interest in the scientific community, as demonstrated by [9, 10, 11], with the ultimate aim of designing optimized materials, able to meet high-tech needs.
In this paper the focus is on reliably evaluating the effective elastic properties of Al_2O_3/ZrO_2, for different volume contents, taking into account the effect of randomness in the micromechanical topology. For this reason we exploit the so-called Fast Statistical Homogenization Procedure in combination with Virtual Element Method, as conceived in [12, 13], to achieve the objective of

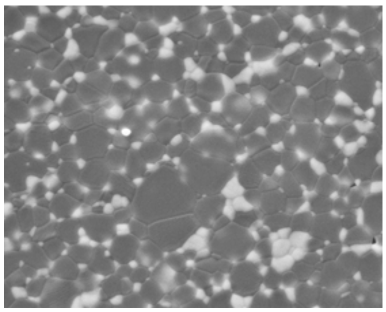

(a) Al_2O_3/ZrO_2(20%-wc); distribution of grain sizes - 0.41 μm $\pm$ 0.22 - Al_2O_3 0.17 μm $\pm$ 0.06 - ZrO_2

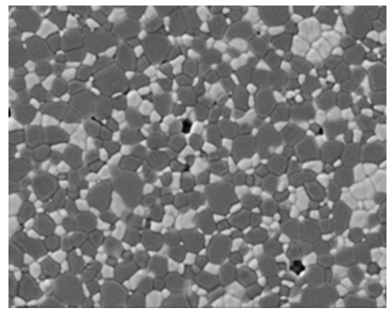

(b) Al_2O_3/ZrO_2(20%-wc); distribution of grain sizes - 0.26 μm $\pm$ 0.11 - Al_2O_3 0.22 μm $\pm$ 0.06 - ZrO_2

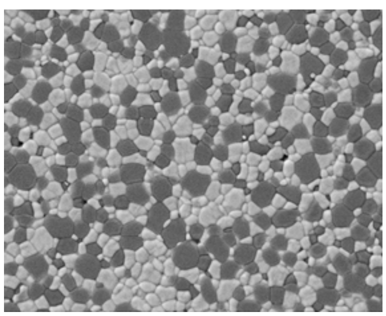

(c) Al_2O_3/ZrO_2(20%-wc); distribution of grain sizes - 0.24 μm $\pm$ 0.07 - Al_2O_3 0.22 μm $\pm$ 0.06 - ZrO_2–

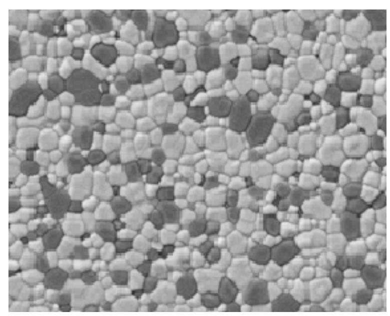

(d) Al_2O_3/ZrO_2(20%-wc); distribution of grain sizes - 0.25 μm $\pm$ 0.07 - Al_2O_3 0.22 μm $\pm$ 0.06 - ZrO_2

Figure 1: Microstructure of analysed ceramic material. Light and dark areas represent ZrO_2 and Al_2O_3, respectively.

a comprehensive elastic characterization of the composites, for a wide range of volume fractions, exploiting a numerical tool that has been proven to be easy to use and fast.
Within the framework of a first order computational homogenization scheme, both the equivalent elastic moduli and the characteristic size of the Representative Volume Element are found by developing bounds of the effective response, obtained by solving Boundary Value Problems with either Dirichlet or Neumann boundary conditions [14, 15], as in [16, 17, 18] in the context of micropolar continua.

Here the numerical strategy of solution is the very recent Virtual Element Method, [19, 20], which has established itself in recent years as a viable alternative to Finite Element Method for a wide range of mechanical applications [21, 22, 23, 24, 25, 26]. One of the key advantages is the high flexibility in the number of nodes and shape of elements, so that it seems a very natural tool for materials with polycrystallyne microstructures [27] since each grain can be discretized with only one virtual element of generic shape. There are other methods in the literature that can deal with polygonal elements to mimic the natural shape of each micro-grain of the material, such as Polygonal Finite Elements [28, 29, 30, 31, 32], Voronoi cell Finite Element Method [33, 34, 35] and Trefftz-Lekhnitskii Grains (TLGs) [36].

The statistical homogenization procedure is based on: i) assuming that the microstructure satisfies the hypothesis of statistical homogeneity and isotropy, combined with the mean-ergodicity; ii) defining realizations of the random composite, sampled in a Monte-Carlo sense, defined as Statistical Volume Elements of increasing characteristic sizes; iii) solving properly conceived boundary problems and evaluating overall mechanical information related both to arithmetic mean and dispersion of results; iv) repeating the procedure up to a convergence criterion is satisfied.
Numerical examples are first devoted to a parametric analysis aimed at characterizing the Al_2O_3/ZrO_2 composite for a set of volume contents ranging from (20%) Al_2O_3/(80%) ZrO_2 up to (80%) Al_2O_3/(20%) ZrO_2. Afterwards a comparison between numerical and experimental results, collected in [8], confirms the reliability of the proposed procedure.
The paper is organized as follows. Section 2 presents an overview of the Fast Statistical Homogenization procedure. In Section 3 numerical examples are presented and critically discussed. Finally in Section 4 conclusions are drawn.

2. Fast Statistical Homogenization Procedure (FSHP)

The main aim of this section is to retrace the so–called Fast Statistical Homogenization Procedure (FSHP), already developed by the authors in [12, 13] for particulate composites with circular inclusions, and here modified for taking into account the peculiar structure of the CMC composites characterised by random geometry of the particles besides random positions. The original statistical procedure has been, indeed, conceived for a particular topology, i.e. composites made of circular inclusions, representative of fibers, randomly dispersed in a second phase, called matrix (Fig. 2(a)). Afterword, it has been adapted to model polycrystalline materials bounded by thin interfaces in which the grains and interfaces zone play the role of inclusions and the matrix, respectively (Fig. 2(b)). Here, focus is on modelling the micro-structure of bi-phase polycrystalline material (Fig. 2(c)).
In what follows, the key ideas of the statistical homogenization procedure are briefly summarized and specialized to the materials at hand.

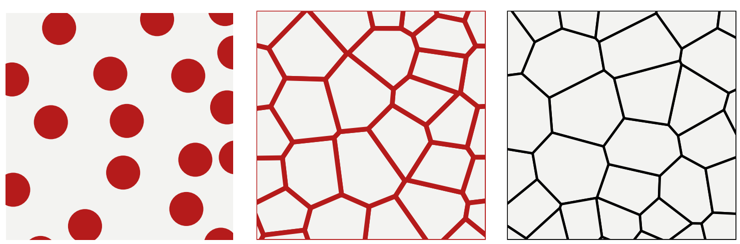

(a) Two-phase material with dispersed fibers (in red) (b) Polycrystal material with thin interfaces (in red) (c) CMC materials

Figure 2: Different models of heterogeneous material taken into account by FSHP.

2.1. First order computational homogenization

A classical energy-based computational homogenization approach [37, 38] is used in combination with the Virtual Element Method to estimate the components of the overall elastic tensor related to realizations of the random CMC Alumina/Zirconia.
In order to perform the homogenization, we describe the material at two

scales of interest: the microscopic and the macroscopic levels. At the microscopic level, the heterogeneous material is represented in detail, accounting for each constituent in terms of geometry and constitutive behaviour. At the macroscopic level the composite material is ideally replaced by an equivalent material whose global behaviour is representative of the actual heterogeneous material. The governing equations are formally the same as those defined at the microscopic level, except for the constitutive law that is not 'a priori' defined at the macroscopic level, but directly descends from the lower level as result of the homogenization procedure. In the following, lower case letters are always related to the micro-scale, while upper case letters to the macro-scale.

In the present case of non periodic composite materials and in view of the statistical homogenization procedure, it is useful to introduce a scale parameter $\delta = L/\overline{d}$ defined, at the microscopic scale, as the ratio between the edge of a square test window L, and the characteristic dimension $\overline{d}$ of a grain. We refer to a linearized two-dimensional framework. At the lower level each material phase is characterized by linear elastic isotropic behaviour with the stress–strain relations written as:

$$\boldsymbol{\sigma} = 2\mu\, \boldsymbol{\varepsilon} + \lambda\, \mathrm{tr}\,(\boldsymbol{\varepsilon})\, \boldsymbol{I} \tag{1}$$

where $\boldsymbol{\varepsilon}$ and $\boldsymbol{\sigma}$ are micro-strain and micro-stress tensors, λ and μ are the Lamé constants, and $\boldsymbol{I}$ is the identity matrix. At the macroscopic level, the general anisotropic stress–strain relations, read:

$$\boldsymbol{\Sigma} = \mathbb{C}\boldsymbol{E}\,, \tag{2}$$

where $\boldsymbol{E}$, $\boldsymbol{\Sigma}$ are the macro-strain and macro-stress tensors and $\mathbb{C}$ is the homogenized material fourth order tensor that contains the homogenized moduli:

$$\mathbb{C} = \left[\begin{array}{ccc} \mathbb{C}_{1111} & \mathbb{C}_{1122} & \mathbb{C}_{1112} \\ \mathbb{C}_{2211} & \mathbb{C}_{2222} & \mathbb{C}_{2212} \\ \mathbb{C}_{1211} & \mathbb{C}_{1222} & \mathbb{C}_{1212} \end{array} \right]\,, \tag{3}$$

i.e. the components of the macroscopic elastic tensor obtained via a homogenization procedure based on the Hill macro-homogeneity condition [39]:

$$\boldsymbol{\Sigma} \cdot \boldsymbol{E} = \frac{1}{A_\delta} \int_{\mathcal{B}_\delta} \boldsymbol{\sigma} \cdot \boldsymbol{\varepsilon}\, dA\,, \tag{4}$$

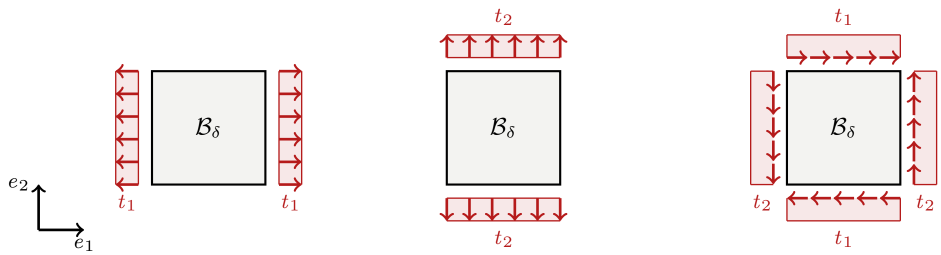

Figure 3: Neumann boundary conditions applied on the window $\mathcal{B}_\delta$

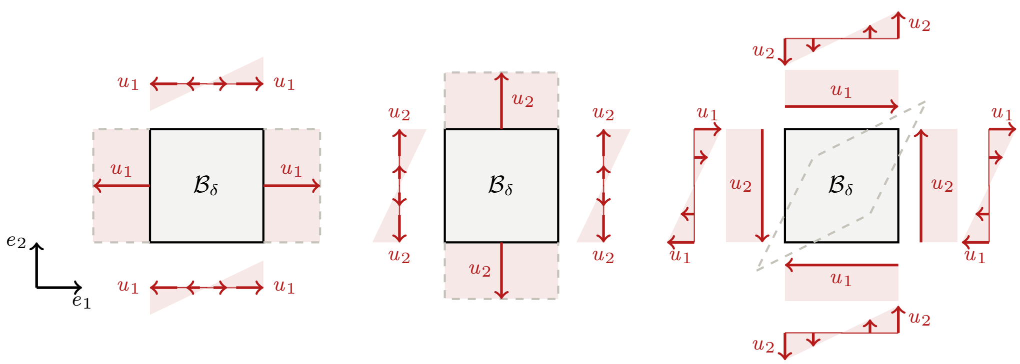

Figure 4: Dirichlet boundary conditions applied on the window $\mathcal{B}_\delta$

which states an energy equivalence between the macroscopic point and the corresponding domain (test window), $\mathcal{B}_\delta$, occupying a region of area A_δ at the microscopic level.

The homogenization procedure is based on the solution of properly defined boundary value problems at the microscopic level with Dirichlet (Fig. 4) and Neumann (Fig. 3) boundary conditions on the boundary $\partial\mathcal{B}_\delta$, directly deriving from the fulfilment of the macro-homogeneity condition, Eq. (4). We focus on a 2-D problem and assume plane strain conditions. The Dirichlet and Neumann BCs reads, respectively:

$$\begin{aligned} \boldsymbol{u} &= \boldsymbol{E}\,\boldsymbol{x}, \quad \text{on} \quad \partial\mathcal{B}_\delta \\ \boldsymbol{t} &= \boldsymbol{\Sigma}\,\boldsymbol{n}, \quad \text{on} \quad \partial\mathcal{B}_\delta \end{aligned} \tag{5}$$

$\boldsymbol{u}$ being the displacement vector and $\boldsymbol{x}$ the coordinates of the generic point on the boundary, $\partial\mathcal{B}_\delta$, with respect to a reference system with origin in the geometric center of the test window $\mathcal{B}_\delta$. $\boldsymbol{t}$ is the traction vector and $\boldsymbol{n}$ the outward normal to $\partial\mathcal{B}_\delta$.

As already shown in [27], the geometrical features of a polycristalline material are particularly suitable for using the Virtual Element Method as a numerical tool for solving Boundary Value Problems at the microscopic scale. In this case, indeed, the microstructure can be satisfactorily modeled with a randomly generated centroidal Voronoi tessellation (CVT) and it can be directly used as a computational mesh. As is well known, in fact, the recent numerical tool of the VEM permits to use single polygonal element for the grains (Fig. 5b), avoiding internal meshing, with consequent high reduction of the computational burden with respect to finite elements.
Note that at this stage, for the sake of simplicity, the average dimension $\overline{d}$ of grains is kept constant, but a straightforward modification to account for different sizes is possible. The computational strategies adopted are aimed

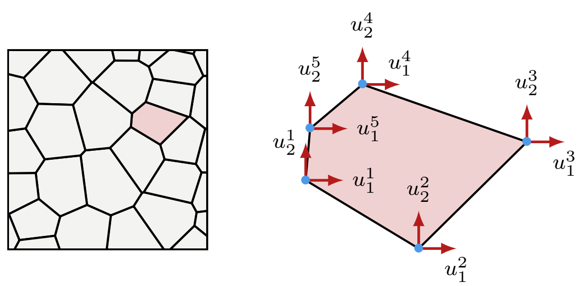

Figure 5: Example of microstrucure modelled via CVT (left) obtained by `PolyMesher` [40] and Virtual Element extract to the mesh (right)

at making the statistical homogenization process as efficient as possible for solving a series (hundreds) of boundary value problems (BVPs), required by the statistical homogenization procedure and to rapidly converge to the RVE solution. The capability of the VEM in delivering reliable estimations of overall elastic moduli, despite the use of very coarse meshes (with consequent important savings in terms of computational burden), has been already assessed in [27, 12].

2.2. Statistical Homogenization

FSHP is based on the statistical homogenization procedure proposed in [41], then developed for micropolar continua in [17] and recently automatized in [12, 13] and briefly described in Section 1.

The proposed homogenization procedure is conceived both for evaluating the homogenized elastic parameters of a non–periodic heterogeneous material, and for identifying the Representative Volume Element (RVE), that in the absence of a repetitive micro-structure is not known a priori.

According to the approach presented in [17], as well as in [42, 43], it is assumed the hypothesis of statistical homogeneity and isotropy combined with the mean-ergodicity of the microstructure. In this framework, the presented procedure requires the statistical definition of a number of realizations called Statistical Volume Elements (SVEs), representing the micro-structure, sampled in a Monte Carlo sense, which allows for determining series of scale–dependent upper and lower bounds for the overall elastic moduli and to approach the RVE size, δ_{RVE}, using a statistical stopping criterion, which is based on the variation of the average elastic moduli.

All steps of the homogenization procedure are completely integrated in the FSHP and they are described below.

Step 1 Input: Set the average dimension of the grains $\overline{d}$ and define the dimensionless scale factor $\delta = L/\overline{d}$. Fix the mechanical parameters of each phase: Young modulus and Poisson coefficients of each phase E_i and ν_i , i=1,2. Set the minimum number of simulations for convergence, N^{lim}, and a tolerance parameter, Tol, based on data dispersion, as defined in above.

Step 2 Input: initialize the window size, $L = L_0$, and number of simulations, $N = N_0$.

Step 3 Realizations: generate a random polygonal mesh with average dimension of grains $\overline{d}$ calling the available `MATLAB`® program `PolyMesher` developed by [40]. Each realization is supposed to be independent from any previous one. Based on volume fractions, mechanical parameters are randomly assigned to grains. In order to avoid abnormal boundary layers related to the artifact of generating the Voronoi tesselations from realizations of homogeneous random point fields created only within the considered test windows, we generate the realizations used in the numerical simulations by cutting out smaller windows. Examples of realization of the micro-structure and the related generated mesh for circular and polycrystal inclusions are shown in Figs. 2(a)-2(b). In Fig. 6 a realization obtained by FSHP for different windows size has been plotted, highlighting in red the cutting windows.

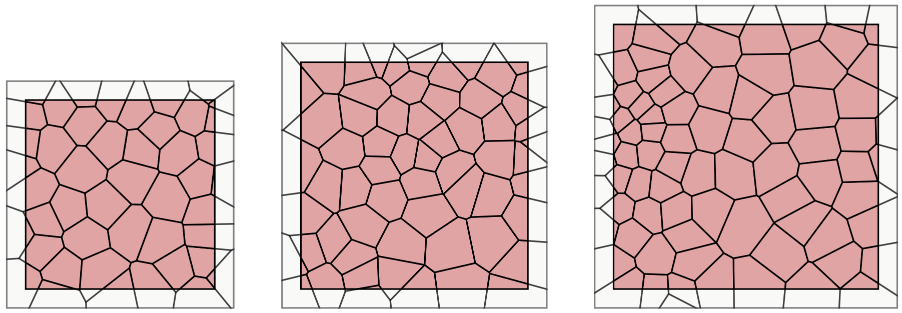

(a) $\delta = 5$ (b) $\delta = 6$ (c) $\delta = 7$

Figure 6: Example of realizations obtained by FSHP for different window size $\delta = L/\bar{d}$ with in red highlighted the cutting windows.

Step 4 Generate/Solve: for each SVE, generate the relative mesh and solve both the Dirichlet and Neumann (Eq. (5)) BVP, and compute the homogenized constitutive parameters.

Step 5 Compute: the bulk modulus

$$\mathbb{K} = \left((\mathbb{C}_{1122} + \mathbb{C}_{2211})/2 + \mathbb{C}_{1212} \right)/6 \,,$$

evaluate the average bulk modulus, $\langle \mathbb{K} \rangle_\delta$, the relative standard deviation $\sigma(\langle \mathbb{K} \rangle_\delta)$ and variation coefficient $CV(\langle \mathbb{K} \rangle_\delta)$. Then compute

$$N_i = (1.96\, \sigma(\langle \mathbb{K} \rangle_\delta)/(\langle \mathbb{K} \rangle_\delta\, Tol)^2 \,, \tag{6}$$

which ensures that the confidence interval of the average homogenized constitutive parameter set at 95%, evaluated over the normal standard distribution, is within the tolerance allowed, Tol. Repeat Steps 3-4 until $N_i \leqslant N^{lim}$.

Step 6 Checking: if the number of realizations necessary for ensuring the requirement at Step 5 is small enough, stop the procedure. We choose as the number of realizations necessary the largest unfavourable number between those obtained by solving BVPs of Neumann or Dirichlet. Otherwise choose an increased value of δ and go to Step 3.

The fulfilment of the requirement at Step 6 means that the values of the homogenized constitutive coefficients are distributed around their averages with a vanishing variation coefficient, and that the RVE size is achieved. The effective homogenized elastic moduli can be determined as the arithmetic mean value between the Dirichlet (upper) and Neumann (lower) bounds at the convergence window (RVE).

The statistical convergence criterion adopted is based on a 95% confidence level of the Normal Standard distribution, which provides the number N of realizations at which it is possible to stop the simulations for a given window size δ. When this number is small enough, the average values of the effective moduli converge and the RVE size is achieved. This circumstance also corresponds to reaching the minimum window size δ_{RVE} for which the estimated homogenized moduli remain constant, within a tolerance interval less than 0.5% for both the Dirichlet and Neumann solutions. The minimum number of simulations, N^{lim}, and the tolerance parameter, Tol, are chosen in order to define a narrow confidence interval for the average and to obtain a reliable convergence criterion. The adopted statistical criterion allows us to detect the RVE size also when the Dirichlet and Neumann solutions do not tend to the same value. The values of the tolerance are assumed as a function of the data dispersion [17].

3. Identification of Alumina/Zirconia properties

This session is devoted to numerical applications aimed both at characterizing the elastic properties of the polycrystalline composite at hand for different contents of Alumina/Zirconia and at identifying the dimension of the RVE. In Section 3.1 a parametric analysis is carried out and elastic homogenized moduli are directly compared with classical upper and lower bound estimates. Section 3.2, on the other hand, presents a comparison with experimental results in [8].

3.1. Comparison with Voigt and Reuss bounds

The Fast Statistical procedure is applied to characterize the elastic response of the Alumina/Zirconia CMC material in terms of first order homogenized moduli taking into account the influence of randomness in the microstructural topology. Results are compared with the well known upper (Voigt) and lower (Reuss) bounds estimated using the so-called rule of mixture and inverse rule of mixture, respectively.

Table 1: Properties of Al_2O_3 and ZrO_2 at room temperature as in [44]

Composite component	E [GPa]	ν [/]
Al_2O_3	400	0.22
ZrO_2	200	0.25

Each phase is assumed to behave as a homogeneous linear elastic material. Their properties, borrowed from [44], are reported in Table1. Regarding the dimension of the grains, here we assumed an average dimension $\overline{d} = 5\mu m$. We consider four different $\mathrm{Al_2O_3/ZrO_2}$ composites characterized by volume fraction $\rho_{Al_2O_3}$ of Alumina in the range 20% to 80%. Figure 7 shows an example of realizations corresponding the four type of materials examined for the window $\delta = 8$. From the homogenization procedure it emerges that the overall behaviour of the composite material does not significantly differ from that of an equivalent isotropic material. In Figure 8(a) and (b) the Dirichlet and the Neumann solutions in terms of homogenized bulk modulus $\langle \mathbb{K} \rangle$ are plotted considering the four values of volume fractions and for different window sizes δ ranging from 5 to 10. As expected, the material tends to become stiffer as the volume content of alumina increases. Dirichlet and Neumann solutions deliver upper and lower bounds, respectively. Applying the convergence criterion in Eq. 6, it emerges that results reach the convergence values at $\delta = 10$, corresponding to the dimension of the RVE. Note that, due to the low material contrast between alumina and zirconia small variations of $\langle \mathbb{K} \rangle$ are observed as δ increases. Moreover, the convergence trend for the different materials depends on the different dispersion of results, as shown in Figs. 9, where the Coefficient of Variation, CV, is plotted versus δ for Dirichlet (blue solid line) and Neumann (red solid line) solutions. As the volume fraction of alumina increases, with the same window size lower values of CV are reached for both Dirichlet and Neumann boundary conditions. The reliability of the proposed procedure is verified by comparing the obtained homogenized moduli with results of well established rule of mixture and inverse rule of mixture, providing upper and lower bounds of homogenized elastic moduli. Considering the homogenized bulk modulus and the composite alumina-zirconia composite characterized by alumina volume fraction $\rho_{Al_2O_3}$, the upper bound

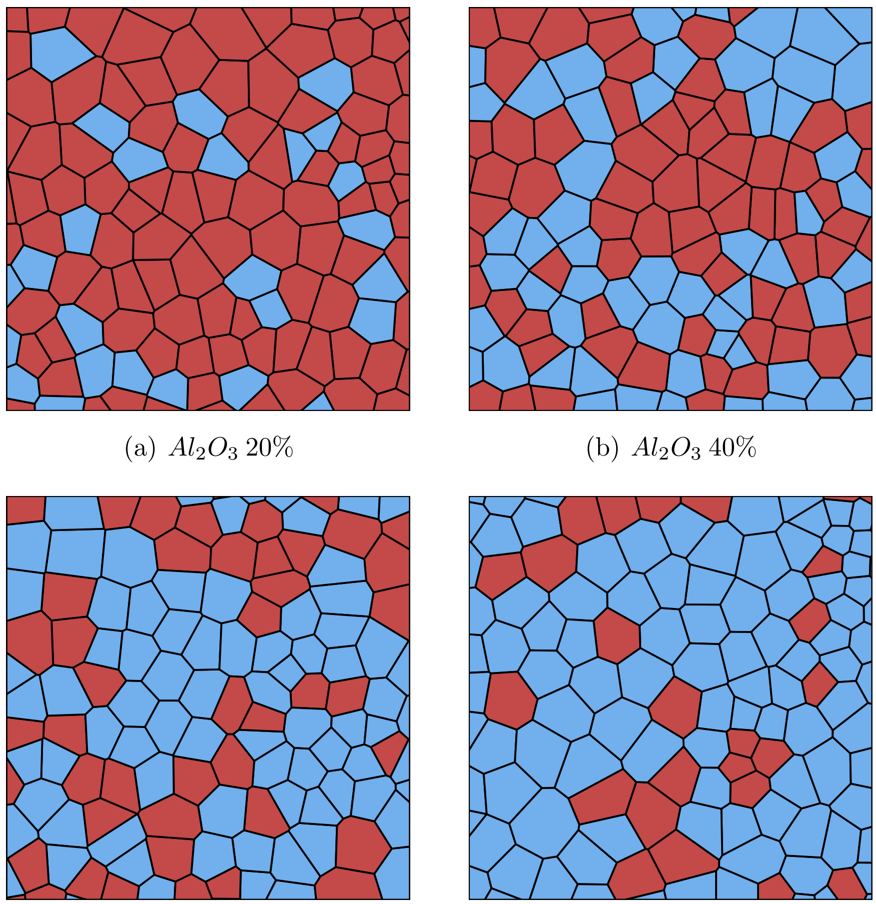

(a) Al_2O_3 20%

(b) Al_2O_3 40%

(c) Al_2O_3 60%

(d) Al_2O_3 80%

Figure 7: Example of realization with different level of Alumina Al_2O3 and Zirconia ZrO_2 for window dimension $\delta = L/\overline{d} = 9$: Alumina and Zirconia grains are depicted in blue and red color, respectively

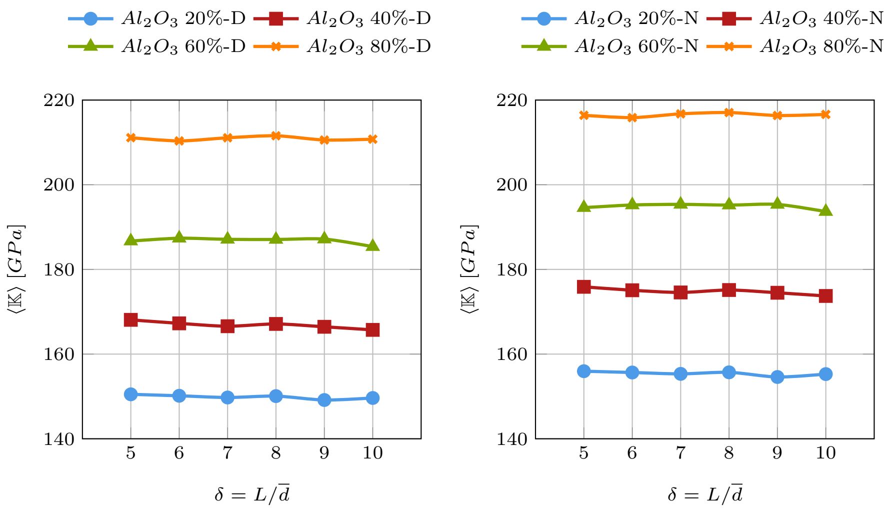

(a) Dirichlet boundary conditions (b) Neumann boundary conditions

Figure 8: Homogenized Bulk modulus $\langle\mathbb{K}\rangle$ with varying the window dimension $\delta = L/\overline{d}$

solution, obtained using the Voigt model, results as

$$\langle\mathbb{K}\rangle^{upper}_{Al_2O_3/ZrO_2} = \langle\mathbb{K}\rangle_{Al_2O_3}\rho_{Al_2O_3} + \langle\mathbb{K}\rangle_{ZrO_2}(1-\rho_{Al_2O_3}) \tag{7}$$

as well as the lower bound solution, obtained via the Reuss model, reads as

$$\langle\mathbb{K}\rangle^{lower}_{Al_2O_3/ZrO_2} = \left(\frac{\rho_{Al_2O_3}}{\langle\mathbb{K}\rangle_{Al_2O_3}} + \frac{1-\rho_{Al_2O_3}}{\langle\mathbb{K}\rangle_{ZrO_2}}\right)^{-1} \tag{8}$$

In Figure 10 the values of homogenized bulk modulus corresponding to RVEs are plotted as the volume content of alumina varies. The extremal cases correspond to pure zirconia and pure alumina. Blue and red curves are referred to Dirichlet and Neumann solutions obtained with the Fast Statistical Homogenization procedure, while dashed black and orange curves are referred to upper and lower bounds resulting from rule of mixture and inverse rule of mixture, respectively. As expected, it is observed that the results obtained from the proposed homogenization procedure fall within the bounds.

Furthermore, the same investigation has been carried out considering the homogenized Poisson's ratio corresponding to the RVE. As emerges from Figure 11, where the four curves have the same meaning as in Figure 10, slight

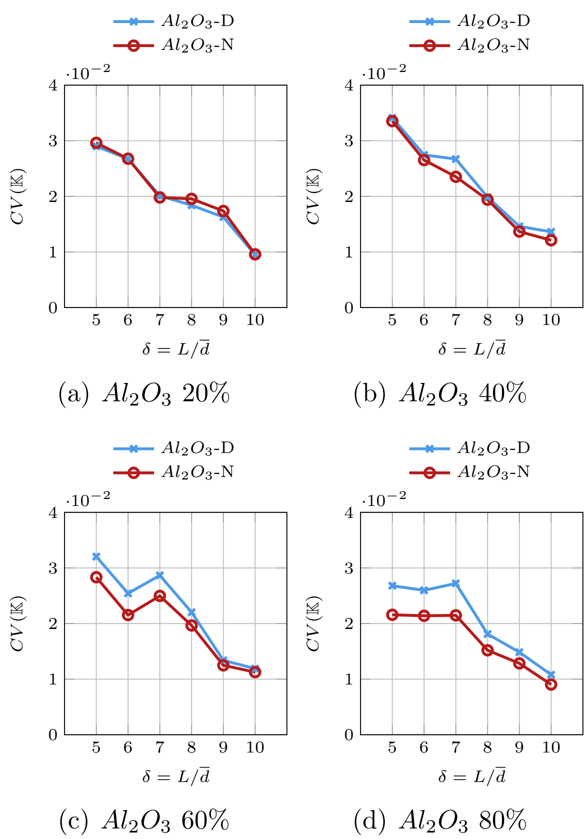

(a) Al_2O_3 20% (b) Al_2O_3 40%

(c) Al_2O_3 60% (d) Al_2O_3 80%

Figure 9: Coefficient of variation CV($\mathbb{K}$) for different contents of Al_2O_3: Dirichlet boundary condition in blue line and Neumann boundary conditions in red line

deviations from the upper and lower bounds are observed pointing out that the proposed statistical procedure confirms to provide reliable results.

3.2. Comparison with experimental results

As a second investigation, the numerical procedure is validated against experimental results of [8] corresponding to four different alumina/zirconia composites. In the referred paper a comprehensive experimental campaign has been carried out with the aim of determining a wide set of material properties as fracture toughness, bending strength, Young's modulus, hardness and subcritical crack growth. Examples of tests performed in the Lublin laboratories are shown in Fig.12. In this context, we are interested in homogenized Young modulus. In line with [8], we consider for the alumina, Al_2O_3,

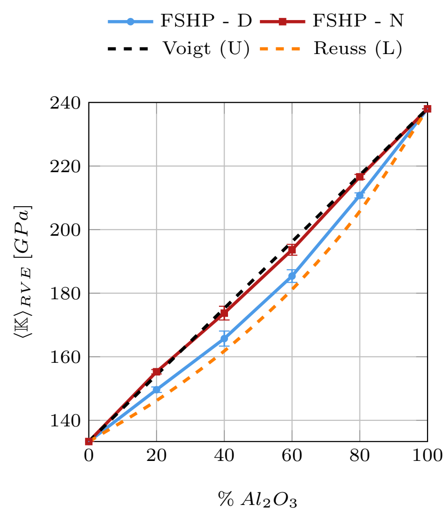

Figure 10: Homogenized Bulk modulus $\langle \mathbb{K} \rangle_{RVE}$ at convergence for different level of percentage ρ of Al_2O_3

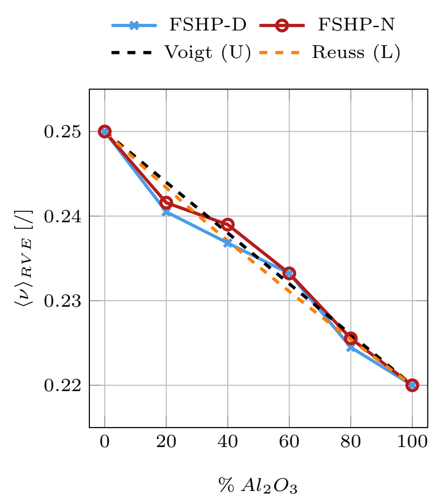

Figure 11: Homogenized Poisson coefficient $\langle \nu \rangle_{RVE}$ at convergence for different level of percentage ρ of Al_2O_3

Young modulus $E = 370$ GPa and Poisson's ratio $\nu = 0.22$, while for zirconia, ZrO_2, Young modulus $E = 205$ GPa and Poisson's ratio $\nu = 0.25$. In Fig-

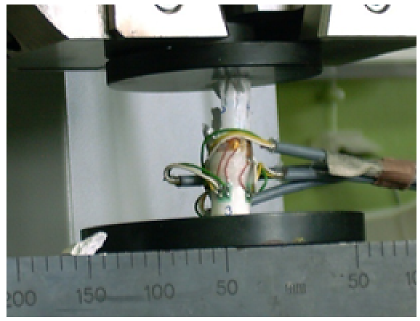

(a) Compression test

(b) Example of the specimen

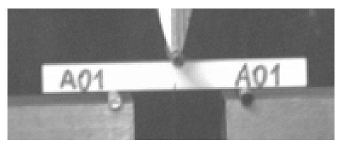

(c) Three bending point test

Figure 12: Example of tests campaign performed at Lublin laboratories [8].

ure 13 the homogenized Young moduli as the volume content of Al_2O_3varies are plotted considering both experimental results and those obtained via the numerical statistical procedure at hand. A very good agreement is found, confirming that the FSHP is able to accurately reproduce experimental results.

Finally, in Table 2 the homogenized average components $\mathbb{C}_{ijhk}$ of the elastic fourth order tensor, corresponding to the RVE, are listed for the four values of Al_2O_3 content. As already mentioned, the overall elastic behaviour can be described with a good approximation by an isotropic linear elastic equivalent continuum.

4. Final remarks

The polycrystalline Al_2O_3/ZrO_2 composite [8] has been characterized in the linear elastic regime by generalizing a statistical homogenization procedure previously developed by some of the authors [12, 13]. Emphasis is placed on the influence that randomness in the phase distribution can have on the equivalent elastic response of the polycrystalline material. The procedure

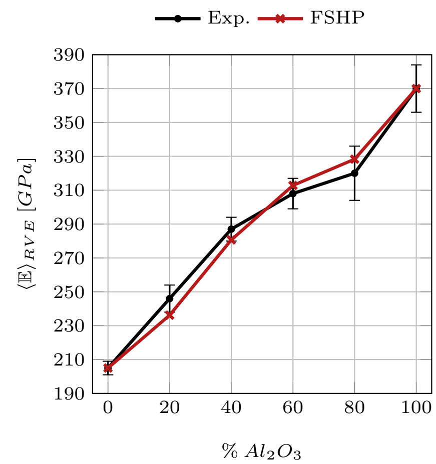

Figure 13: Homogenized Young modulus $\langle E \rangle_{RVE}$ at convergence for different level of percentage ρ of Al_2O_3 (red line) versus experimental test (black line)

has the twofold purpose of estimating the elastic moduli via upper and lower bounds obtained with Dirichlet and Neumann type boundary conditions and identifying the dimension of the RVE corresponding to the composite material. The numerical tool exploited to solve boundary value problems is the recent Virtual Element Method.
Numerical investigations are carried out accounting for different phase contents in the composite ranging from pure Alumina to pure Zirconia. A first investigation highlights that as expected the Neumann and Dirichlet bounds obtained with the proposed solution fall within upper and lower bounds ob-

Table 2: Homogenized elastic parameters of Al_2O_3/ZrO_2 composite for different level of alumina Al_2O_3 percentage

% Al_2O_3 [/]	$\mathbb{C}_{1111}$ [GPa]	$\mathbb{C}_{1122}$ [GPa]	$\mathbb{C}_{2211}$ [GPa]	$\mathbb{C}_{2222}$ [GPa]	$\mathbb{C}_{1212}$ [GPa]
20	279.1555	89.2250	89.2090	279.0855	192.8280
40	306.4810	95.0085	94.9825	307.1135	215.4210
60	362.2085	106.5220	106.5265	361.3640	257.8255
80	377.9210	109.9360	109.9520	377.1985	269.9895

tained with Voigt and Reuss models. Given the low contrast between the elastic modules of two phases, the procedure guarantees convergence for relatively small testing windows, corresponding to RVEs of rather small dimensions, i.e. with a characteristic size equal to approximately 10 times the average grain size. Moreover, it is noted that the homogenized material exhibits an overall elastic response that does not significantly differ from the isotropic behaviour.
The numerical procedure has been, then, successfully applied to reproduce experimental results related to characterization of Young modulus for a set of Alumina/Zirconia materials which differ in Alumina content.
Further developments envisage the investigation of homogenized non-linear constitutive behaviors, possibly accounting for crack onset and development.

5. Acknowledgements

The results presented in this paper were obtained within the framework of research grant No. UMO/2016/21/B/ST8/01027 financed by the National Science Centre, Poland. This work is supported by Italian Ministry of University and Research (P.R.I.N. National Grant 2017 No. 2017HFPKZY (B88D19001130001); Sapienza Research Grants "Progetti Grandi" 2021 ().

References

[1] A. Okada, Automotive and industrial applications of structural ceramics in japan, Journal of the European Ceramic Society 28 (5) (2008) 1097–1104.

[2] F. Christin, Cmc materials for space and aeronautical applications, Ceramic matrix composites: fiber reinforced ceramics and their applications (2008) 327–351.

[3] W. Krenkel, Ceramic matrix composites: fiber reinforced ceramics and their applications, John Wiley & Sons, 2008.

[4] F. Raether, Ceramic matrix composites- an alternative for challenging construction tasks, Ceramic Applications 1 (1) (2013) 45–49.

[5] P. Spriet, Cmc applications to gas turbines, Ceramic matrix composites: materials, modeling and technology (2014) 591–608.

[6] V. Naglieri, P. Palmero, L. Montanaro, J. Chevalier, Elaboration of alumina-zirconia composites: Role of the zirconia content on the microstructure and mechanical properties, Materials 6 (5) (2013) 2090–2102.

[7] T. Sadowski, L. Marsavina, Multiscale modelling of two-phase ceramic matrix composites, Computational Materials Science 50 (4) (2011) 1336–1346.

[8] M. Boniecki, T. Sadowski, P. Golebiewski, H. Weglarz, A. Piatkowska, M. Romaniec, K. Krzyzak, K. Losiewicz, Mechanical properties of alumina/zirconia composites, Ceramics International 46 (1) (2020) 1033–1039. doi:10.1016/j.ceramint.2019.09.068.

[9] T. Sadowski, Gradual degradation in two-phase ceramic composites under compression, Computational materials science 64 (2012) 209–211.

[10] T. Sadowski, B. Pankowski, Numerical modelling of two-phase ceramic composite response under uniaxial loading, Composite Structures 143 (2016) 388–394.

[11] T. Sadowski, K. Łosiewicz, M. Boniecki, M. Szutkowska, Assessment of mechanical properties by nano-and microindentation of alumina/zirconia composites, Materials Today: Proceedings 45 (2021) 4196–4201.

[12] M. Pingaro, E. Reccia, P. Trovalusci, R. Masiani, Fast statistical homogenization procedure (FSHP) for particle random composites using virtual element method, Computational Mechanics 64 (1) (2019) 197–210. doi:10.1007/s00466-018-1665-7.

[13] M. Pingaro, E. Reccia, P. Trovalusci, Homogenization of Random Porous Materials With Low-Order Virtual Elements, ASCE-ASME Journal of Risk and Uncertainty in Engineering Systems, Part B: Mechanical Engineering 5 (3) (2019). doi:10.1115/1.4043475.

[14] V. Eremeyev, J.-F. Ganghoffer, V. Konopińska-Zmysłowska, N. Uglov, Flexoelectricity and apparent piezoelectricity of a pantographic micro-bar, International Journal of Engineering Science 149 (2020). doi:10.1016/j.ijengsci.2020.103213.

[15] N. Mawassy, H. Reda, J.-F. Ganghoffer, V. Eremeyev, H. Lakiss, A variational approach of homogenization of piezoelectric composites towards piezoelectric and flexoelectric effective media, International Journal of Engineering Science 158 (2021). doi:10.1016/j.ijengsci.2020.103410.

[16] P. Trovalusci, M. L. De Bellis, M. Ostoja-Starzewski, A. Murrali, Particulate random composites homogenized as micropolar materials, Meccanica 49 (11) (2014) 2719–2727.

[17] P. Trovalusci, M. Ostoja-Starzewski, M. De Bellis, A. Murrali, Scale-dependent homogenization of random composites as micropolar continua, European Journal of Mechanics, A/Solids 49 (2015) 396 – 407. doi:10.1016/j.euromechsol.2014.08.010.

[18] E. Reccia, M. L. De Bellis, P. Trovalusci, R. Masiani, Sensitivity to material contrast in homogenization of random particle composites as micropolar continua, Composites Part B: Engineering 136 (2018) 39–45.

[19] L. Beirão Da Veiga, F. Brezzi, A. Cangiani, G. Manzini, L. Marini, A. Russo, Basic principles of virtual element methods, Mathematical Models and Methods in Applied Sciences 23 (1) (2013) 199–214. doi:10.1142/S0218202512500492.

[20] L. Beirão Da Veiga, F. Brezzi, L. Marini, Virtual elements for linear elasticity problems, SIAM Journal on Numerical Analysis 51 (2) (2013) 794–812. doi:10.1137/120874746.

[21] P. Wriggers, W. T. Rust, B. Reddy, A virtual element method for contact, Computational Mechanics 58 (6) (2016) 1039–1050.

[22] M. L. De Bellis, P. Wriggers, B. Hudobivnik, G. Zavarise, Virtual element formulation for isotropic damage, Finite Elements in Analysis and Design 144 (2018) 38–48.

[23] F. Aldakheel, B. Hudobivnik, A. Hussein, P. Wriggers, Phase-field modeling of brittle fracture using an efficient virtual element scheme, Computer Methods in Applied Mechanics and Engineering 341 (2018) 443–466.

[24] B. Hudobivnik, F. Aldakheel, P. Wriggers, A low order 3d virtual element formulation for finite elasto–plastic deformations, Computational Mechanics 63 (2) (2019) 253–269.

[25] M. De Bellis, P. Wriggers, B. Hudobivnik, Serendipity virtual element formulation for nonlinear elasticity, Computers & Structures 223 (2019) 106094.

[26] P. Wriggers, M. De Bellis, B. Hudobivnik, A taylor–hood type virtual element formulations for large incompressible strains, Computer Methods in Applied Mechanics and Engineering 385 (2021) 114021.

[27] M. Marino, B. Hudobivnik, P. Wriggers, Computational homogenization of polycrystalline materials with the Virtual Element Method, Computer Methods in Applied Mechanics and Engineering 355 (2019) 349–372. doi:10.1016/j.cma.2019.06.004.

[28] N. Sukumar, A. Tabarraei, Conforming polygonal finite elements, International Journal for Numerical Methods in Engineering 61 (12) (2004) 2045 – 2066, cited by: 353. doi:10.1002/nme.1141.

[29] M. Kraus, A. Rajagopal, P. Steinmann, Investigations on the polygonal finite element method: Constrained adaptive delaunay tessellation and conformal interpolants, Computers and Structures 120 (2013) 33 – 46, cited by: 18. doi:10.1016/j.compstruc.2013.01.017.

[30] J. Bishop, A displacement-based finite element formulation for general polyhedra using harmonic shape functions, International Journal for Numerical Methods in Engineering 97 (1) (2014) 1 – 31, cited by: 93. doi:10.1002/nme.4562.

[31] G. Manzini, A. Russo, N. Sukumar, New perspectives on polygonal and polyhedral finite element methods, Mathematical Models and Methods in Applied Sciences 24 (8) (2014) 1665 – 1699, cited by: 115. doi:10.1142/S0218202514400065.

[32] A. Francis, A. Ortiz-Bernardin, S. P. Bordas, S. Natarajan, Linear smoothed polygonal and polyhedral finite elements, International Journal for Numerical Methods in Engineering 109 (9) (2017) 1263 – 1288, cited by: 64. doi:10.1002/nme.5324.

[33] S. Ghosh, K. Lee, S. Moorthy, Multiple scale analysis of heterogeneous elastic structures using homogenization theory and voronoi cell finite element method, International Journal of Solids and Structures 32 (1) (1995) 27 – 62, cited by: 344. doi:10.1016/0020-7683(94)00097-G.

[34] S. Ghosh, K. Lee, P. Raghavan, A multi-level computational model for multi-scale damage analysis in composite and porous materials, International Journal of Solids and Structures 38 (14) (2001) 2335 – 2385, cited by: 309. doi:10.1016/S0020-7683(00)00167-0.

[35] M. Groeber, S. Ghosh, M. D. Uchic, D. M. Dimiduk, A framework for automated analysis and simulation of 3d polycrystalline microstructures. part 1: Statistical characterization, Acta Materialia 56 (6) (2008) 1257 – 1273, cited by: 241. doi:10.1016/j.actamat.2007.11.041.

[36] P. L. Bishay, S. N. Atluri, Trefftz-Lekhnitskii Grains (TLGs) for efficient Direct Numerical Simulation (DNS) of the micro/meso mechanics of porous piezoelectric materials, Computational Materials Science 83 (2014) 235 – 249, cited by: 13. doi:10.1016/j.commatsci.2013.10.038.

[37] R. Smit, W. Brekelmans, H. Meijer, Prediction of the mechanical behavior of nonlinear heterogeneous systems by multi-level finite element modeling, Computer Methods in Applied Mechanics and Engineering 155 (1-2) (1998) 181 – 192. doi:10.1016/S0045-7825(97)00139-4.

[38] C. Miehe, J. Schröder, J. Schotte, Computational homogenization analysis in finite plasticity simulation of texture development in polycrystalline materials, Computer Methods in Applied Mechanics and Engineering 171 (3-4) (1999) 387 – 418. doi:10.1016/S0045-7825(98)00218-7.

[39] R. Hill, Elastic properties of reinforced solids: Some theoretical principles, Journal of the Mechanics and Physics of Solids 11 (5) (1963) 357 – 372.

[40] C. Talischi, G. Paulino, A. Pereira, I. Menezes, PolyMesher: A general-purpose mesh generator for polygonal elements written in Matlab, Structural and Multidisciplinary Optimization 45 (3) (2012) 309–328. doi:10.1007/s00158-011-0706-z.

[41] M. Sena, M. Ostoja-Starzewski, L. Costa, Stiffness tensor random fields through upscaling of planar random materials, Probabilistic Engineering Mechanics 34 (2013) 131 – 156. doi:10.1016/j.probengmech.2013.08.008.

[42] X. Du, M. Ostoja-Starzewski, On the size of representative volume element for Darcy law in random media, Proceedings of the Royal Society A: Mathematical, Physical and Engineering Sciences 462 (2074) (2006) 2949 – 2963. doi:10.1098/rspa.2006.1704.

[43] M. Ostoja-Starzewski, Microstructural Randomness and Scaling in Mechanics of Materials, CRC Press, Taylor & Francis Group, 2007.

[44] T. Sadowski, Modelling of damage and fracture processes of ceramic matrix composites under mechanical loading, CISM International Centre for Mechanical Sciences, Courses and Lectures 556 (2014) 151–178. doi:10.1007/978-3-7091-1812-2_5.